High sensitivity cavity ring down spectroscopy of N2O near 1.74 μm

Thibault Bertin, Didier Mondelain, Ekaterina Karlovets, S. Kassi, Valery Perevalov, Alain Campargue

High sensitivity cavity ring down spectroscopy of N_2O near 1.74 µm

T. Bertin[1#], D. Mondelain[1], E.V. Karlovets[1, 2,3], S. Kassi [1], V.I. Perevalov[3], A. Campargue[1*]

[1] Univ. Grenoble Alpes, CNRS, LIPhy, 38000 Grenoble, France
[2] Tomsk State University, Laboratory of Quantum Mechanics of Molecules and Radiative Processes, 36, Lenin Avenue, 634050, Tomsk, Russia
[3]Laboratory of Theoretical Spectroscopy, V.E. Zuev Institute of Atmospheric Optics, Siberian Branch, Russian Academy of Sciences,1, Academician Zuev Square, 634055 Tomsk, Russia

Number of pages: 23

Number of tables: 3

Number of figures: 8

Keywords: Nitrous oxide;$^{14}N_2{}^{16}O$; CRDS; Vibration-rotational transitions; Line positions; Line intensities

Master student of the Université Libre de Bruxelles (Belgium) who contributed to this work in the frame of an internship at LIPhy
* *Corresponding author: Alain.Campargue@univ-grenoble-alpes.fr*

Abstract

In spite of being a greenhouse gas with a large global warming potential, the absorption spectrum of nitrous oxide in the near infrared is insufficiently characterized. In the present work, the spectral region near 1.74 μm (5695-5910 cm^{-1}) is investigated by high sensitivity cavity ring down spectroscopy (CRDS).The noise level of the CRDS spectra corresponds to a typical minimum detectable absorption, α_{min}, below 10^{-10} cm^{-1}. 3326 transitions are measured and rovibrationally assigned to 50 bands of five nitrous oxide isotopologues ($^{14}N_2{}^{16}O$, $^{14}N^{15}N^{16}O$, $^{15}N^{14}N^{16}O$, $^{14}N_2{}^{18}O$ and $^{14}N_2{}^{17}O$) in natural isotopic abundance. The weakest lines assigned have an intensity below10^{-28} cm/molecule. For comparison, only three $^{14}N_2{}^{16}O$ bands are included in the HITRAN database in the region, with a 2×10^{-25} cm/molecule intensity cut off. The rovibrational assignments of the spectra were performed by comparison with predictions performed for each isotopologue in the frame of the effective operator approach. The overall quality of the predictions is satisfactory for line positions. Deviations larger than 0.1 cm^{-1} are nevertheless noted for $^{14}N_2{}^{16}O$ and $^{14}N_2{}^{18}O$.

The spectroscopic parameters of the upper level of the observed bands were derived from the standard band-by-band fit of the measured line positions. A significant number of bands were found to be perturbed by local rotational perturbations and in some cases, extra lines due to an intensity transfer could be assigned. The interaction mechanisms and the perturbers were univocally identified on the basis of the effective Hamiltonian model. In particular, interpolyad couplings were evidenced indicating that the polyad version of the effective Hamiltonian has to be extended to include Coriolis and interpolyad anharmonic interactions. No satisfactory modeling of the N_2O line intensities is yet available in the region. The CRDS intensity values derived in this work provides a solid set of measurements for future empirical intensity modeling in the region.

1. Introduction

Nitrous oxide is a powerful greenhouse gas with a Global Warming Potential about 300 times stronger than that of carbon dioxide. Over the last century, the N_2O atmospheric concentration has experienced a steep increase from about 270 ppb to 330 ppb mainly due to anthropogenic sources. The present contribution takes part in a long standing effort to better characterize the absorption spectrum of nitrous oxide in the near and short wavelength infrared. In the last years, high sensitivity absorption spectra were recorded by cavity ring down spectroscopy (CRDS), extending importantly previous observations by Fourier Transform Spectroscopy (FTS). The large 5900-8334 cm^{-1} range (1.7-1.2 µm) was covered using a series of about one hundred fibered distributed feed-back (DFB) laser diodes [1-6] and an external cavity diode laser (ECDL) [7,8]. In the present study, we extend the studied spectral interval to lower energy by covering the 5695-5910 cm^{-1} range using a newly purchased set of DFB laser diodes. The high sensitivity of the recordings (typical noise equivalent absorption of the spectra on the order of α_{min}~ 8×10^{-11} cm^{-1}) allowed us for measuring weak lines with intensities below 10^{-28}cm/molecule. Overall, more than 4300 lines were measured in the studied region. The rovibrational assignments were performed on the basis of the predictions of the effective Hamiltonian models developed for each isotopologue of nitrous oxide present in natural isotopic abundance in the studied sample. As a result more than 3300 transitions belonging to 50 bands could be assigned to five isotopologues ($^{14}N_2{}^{16}O$, $^{14}N^{15}N^{16}O$, $^{15}N^{14}N^{16}O$, $^{14}N_2{}^{18}O$ and $^{14}N_2{}^{17}O$).

After the description of the data acquisition and of the line list construction in the next section, the rovibrational assignments are presented in Section 3. Section 4 is devoted to the band-by-band derivation of the spectroscopic constants of the upper levels and to the analysis of the evidenced rovibrational perturbations. Finally, we discuss in Section 5 the comparison with the line lists calculated in the frame of the effective operator approach.

2. Experimental setup

The reader is referred to Ref. [9] for general description of the CRDS setups developed in our group. The spectra recordings were performed with the CRD spectrometer used recently for investigating the 1.75 µm transparency window of carbon dioxide [10-12]. It is of the same type as the DFB setup used in our previous investigations of nitrous oxide at higher energy [1-6]. Using a set of eight DFB laser diodes (from Eblana Photonics) as light sources, the 5695-5900 cm^{-1} spectra interval is now accessible for our CRDS recordings. Each laser diode tuning ranges about 20 cm^{-1} by temperature tuning from -5°C to 55°C allowing for the coverage of the 5693-5850 cm^{-1} range with only a few spectral gaps: 5714.71-5722.06,

5742.72-5745.47, 5773.38-5778.54, 5847.59-5858.01, 5882.35-5883.52 cm^{-1}. The finesse of the cavity varied from 130,000 at 5850 cm^{-1} to 200,000 at 5700 cm^{-1} resulting in measured ring down (RD) times from 200 µs to 300 µs, respectively. About 30 to 100 RD events were averaged per spectral point.

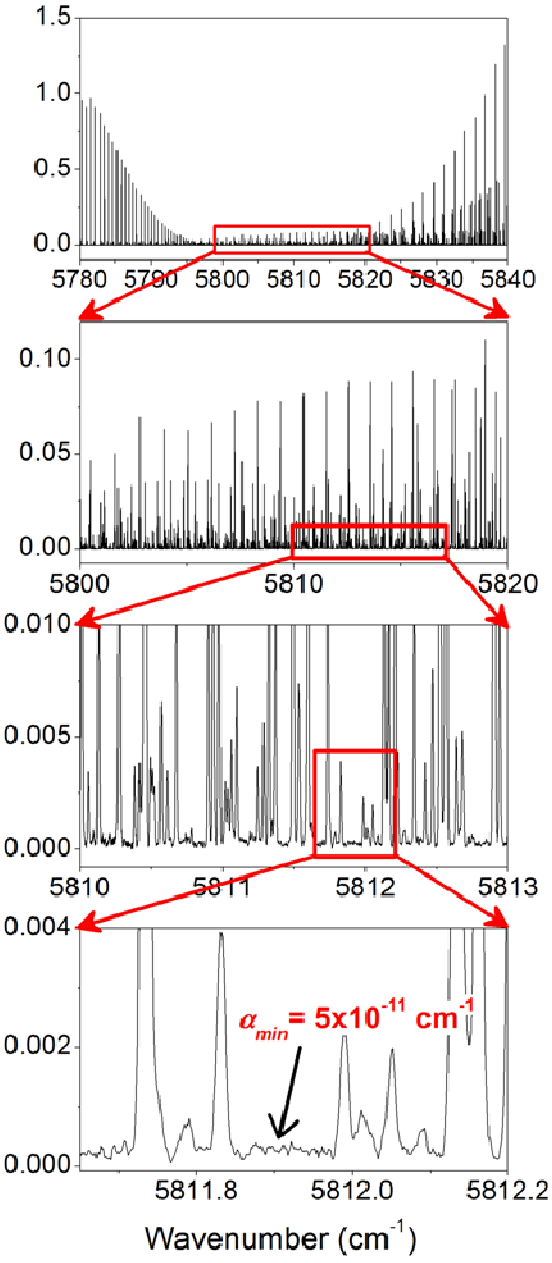

Fig. 1
CRDS spectrum of natural nitrous oxide near 5810 cm^{-1}. The sample pressure was 1.0 Torr. Four successive enlargements illustrate the high dynamics of the recordings giving access to absorption coefficients from 10^{-6} cm^{-1} to the noise level α_{min}~ 5×10^{-11} cm^{-1}.

The cell was filled with N_2O (Alphagaz N40, purity>99.99%) in normal isotopic abundance at a pressure of 1.0 Torr. The cell temperature was measured with a temperature sensor (TSic 501, IST-AG, 0.1 K accuracy) fixed on the cell surface, covered by an external

blanket of foam for thermal isolation. During the recordings reported here, the cell temperature varied between 293.4 and 295.1 K. The gas pressure was continuously measured by a capacitance gauge (MKS Baratron, 10 Torr, 0.25 % accuracy of the reading).

During the spectrum recording, a wavemeter measured the wavenumber of the laser emission at each spectral step of typically 0.002 cm^{-1} giving a first frequency calibration of the spectrum. This calibration was then refined using accurate N_2O line positions provided by the HITRAN2016 database [13]. This leads to an estimated uncertainty of 1×10^{-3} cm^{-1} on the line center determination of unblended lines.

The minimum detectable absorption coefficient (evaluated as the *rms* of the base line fluctuation), α_{min}, varies between 1×10^{-10} $cm^{-1}$and 4×10^{-11} cm^{-1} depending on the RD time. As a result, line intensities spanning four orders of magnitude (from 5×10^{-25} to 5×10^{-29} cm/molecule) could be retrieved from the measured spectra. The successive enlargements of the spectra presented in **Fig. 1** illustrate the sensitivity and high dynamic range of the recordings and the noise level on the order of $\alpha_{min}\sim 5\times10^{-11}$ cm^{-1}. The observed high spectral congestion made the rovibrational assignment particularly laborious.

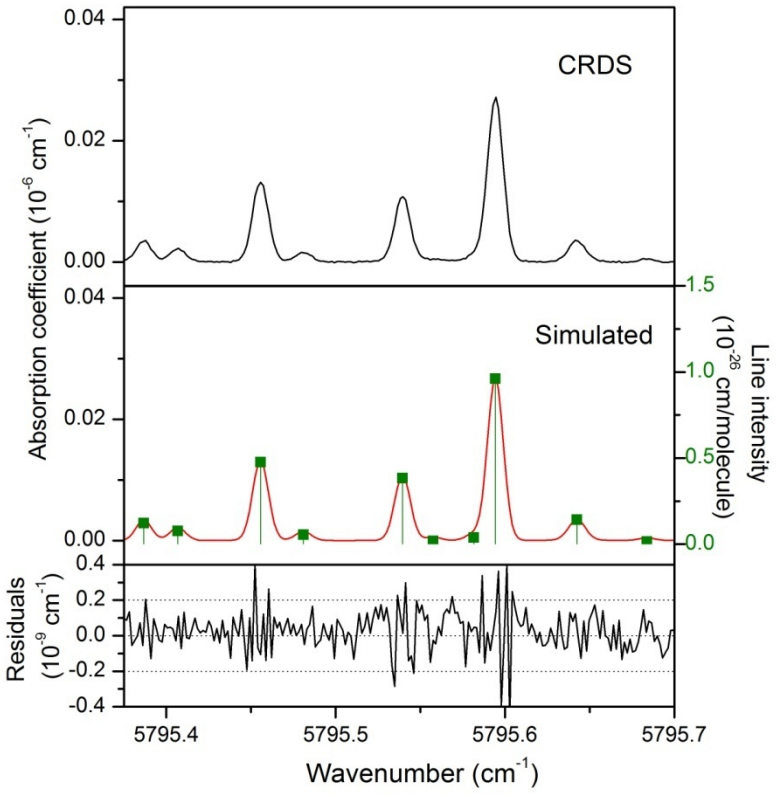

Fig. 2
Fragment of the CRDS (top panel) and simulated (middle panel) room temperature spectra of N_2O recorded at 1 Torr near 5795 cm^{-1}. The residuals between measured and simulated spectra are given in the bottom panel. The stick spectrum in the middle panel corresponds to the retrieved CRDS line list.

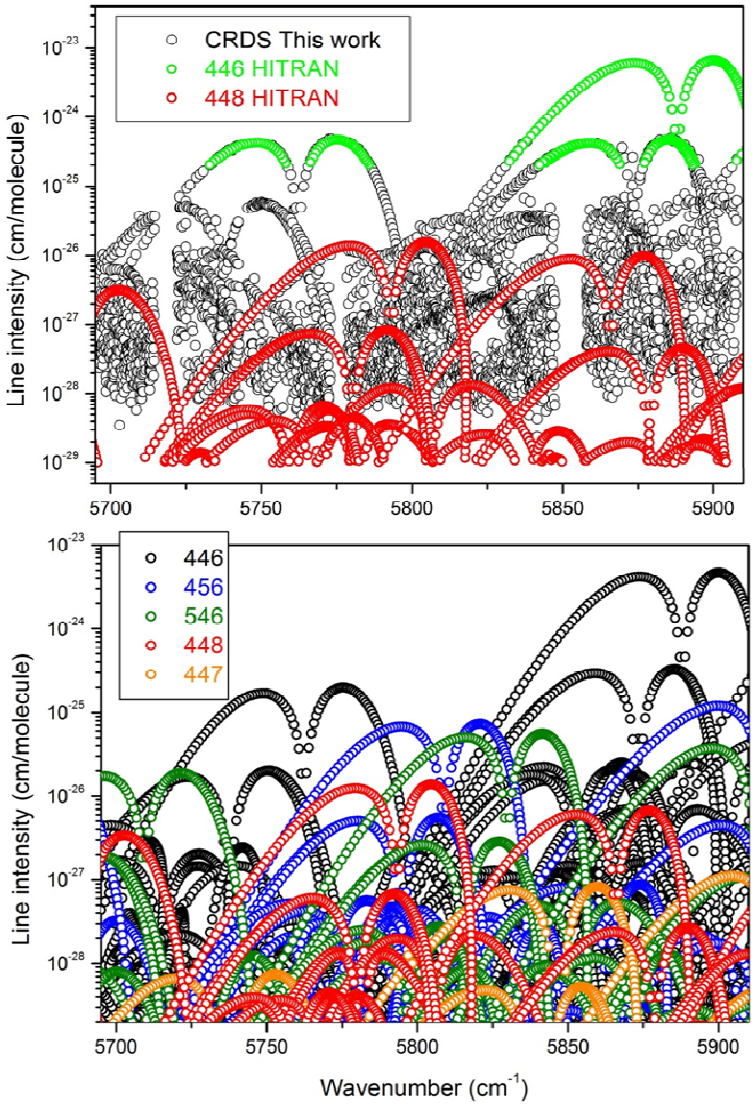

Fig. 3
Overview of the spectrum of N_2O in natural isotopic abundance in the 5695-5910 cm^{-1} region.
Upper panel: CRDS line list (black circles) obtained in this work. The HITRAN line list which is superimposed consists of bands of $^{14}N_2{}^{16}O$ (green) and $^{14}N_2{}^{18}O$ (red). Narrow spectral gaps in the CRDS line list correspond to interval inaccessible with the laser sources at disposal.
Lower panel: Line list predicted within the effective operator approach for the various N_2O isotopologues. Calculated intensities are rough estimations useful for rovibrational assignments (see Text).

The line centres and line intensities were obtained by using a homemade interactive least squares multi-lines fitting code written in LabVIEW. A Voigt profile with the width of the Gaussian component fixed to the calculated Doppler broadening was adopted for each line. At the pressure of the recordings (1 Torr), the self collisional width is less than 10^{-3} cm^{-1} (HWHM) [13]. This value is significantly smaller than the Doppler broadening of 5.3× 10^{-3} cm^{-1}. For the weak lines, the Lorentzian width was fixed by default to HITRAN value but for

the medium and strong lines, significant residuals were observed and the quality of the spectra allowed refining the collisional width. It is difficult to attach individual error bar to the retrieved line intensities. In the case of unblended lines with intensity larger than 3×10^{-26} cm/molecule, we estimate the intensity uncertainty to be better than 5 %. This value can reach 50% for weaker lines in particular when they are blended.

The global line list was obtained by gathering line parameters retrieved from the different recordings. It counts 4337 lines presented in the upper part of **Fig. 3** which also includes the HITRAN2016 line list for comparison. HITRAN line list consists in the strongest bands of the main isotopologue, $^{14}N_2{}^{16}O$ and of the strongest bands of the fourth abundant isotopologue, $^{14}N_2{}^{18}O$. As shown on **Fig. 3**, part of the HITRAN lines of $^{14}N_2{}^{16}O$ are absent from our list. This is due to the fact that they induce a large absorption which results in a very weak transmitted signal by the cavity making the measurement of the ring down time inaccurate. Note that, as a result of the 3.6×10^{-4} isotopic abundance of $^{14}N_2{}^{18}O$, all the bands included in the HITRAN list for this isotopologue have line intensities below the HITRAN intensity cut off of the main isotopologue $^{14}N_2{}^{16}O$ (2×10^{-25}cm/molecule). As a result, the HITRAN line list is thus largely incomplete above the intensity cut off of the $^{14}N_2{}^{18}O$ isotopologue (10^{-29} cm/molecule).

3. Rovibrational assignments

In a first step, the presence of impurity lines in the line list, in particular water vapor lines, was searched. By comparison with the HITRAN database [13], 27 water lines were identified and discarded. The rovibrational assignments were performed on the basis of predictions performed for each isotopologue using the effective operator approach. Predicted line lists were generated using the effective Hamiltonians (EH) and effective dipole moment (EDM) operators. The EH has a polyad structure resulting from the approximate relations $\omega_3\approx 2\omega_1\approx 4\omega_2$ between the harmonic normal mode frequencies. The diagonal blocks are characterized by the polyad number, P, given by $P= 2V_1+V_2+ 4V_3$ where V_1, V_2, and V_3 denote the normal mode vibrational quantum numbers. The EH used for the different isotopologues are presented in the following references: Ref. [14] ($^{14}N_2{}^{16}O$), Ref. [15] ($^{14}N^{15}N^{16}O$), Ref. [16] ($^{15}N^{14}N^{16}O$) and Ref. [8] ($^{14}N_2{}^{18}O$). In the case of the $^{14}N_2{}^{17}O$ isotopologue, a preliminary set of EH parameters fitted to very restricted number of the line positions was used [17].

In the studied region, all but three bands belong to $\Delta P= 10$ series of transitions. Three $^{14}N_2{}^{16}O$ bands (3310-0000, 3420-0110 3400-0110 near 5722.8, 5744.7 and 5784.5 cm^{-1}, respectively) belong to the $\Delta P= 9$ series. In principle, the calculations of the line intensities

within the effective operator approach require EDM parameters for each ΔP series and *for each isotopologue*. This is particularly true in the case of N_2O where interpolyad couplings strongly impact the band intensities and differ importantly between the different isotopologues. In the present case, the required sets of ΔP= 9 and 10 EDM parameters are only available for the main isotopologue [18,19] which makes the predictions of the line intensities of the minor isotopologues quite hazardous. Nevertheless, although not accurate, intensity predictions are needed for rovibrational assignments based on the comparison of the experiment to the predictions. This is why, the EDM parameters of $^{14}N_2{}^{16}O$ were used to compute line intensities for all the isotopologues.

The overview of the resulting predicted line list for N_2O in natural isotopic abundance is compared to the CRDS line list in **Fig. 3**. The level of agreement observed at the scale of the overview does not hold at a detailed scale, in particular for line intensities. Nevertheless, in spite of their rough accuracy, the line intensity criterion was crucial in the assignment process. The assignments of the $^{14}N^{15}N^{16}O$ and $^{15}N^{14}N^{16}O$ lines were made easier by the fact that the line position predictions are accurate as they reproduce FTS measurements obtained with enriched species [15,20] which include our observations.

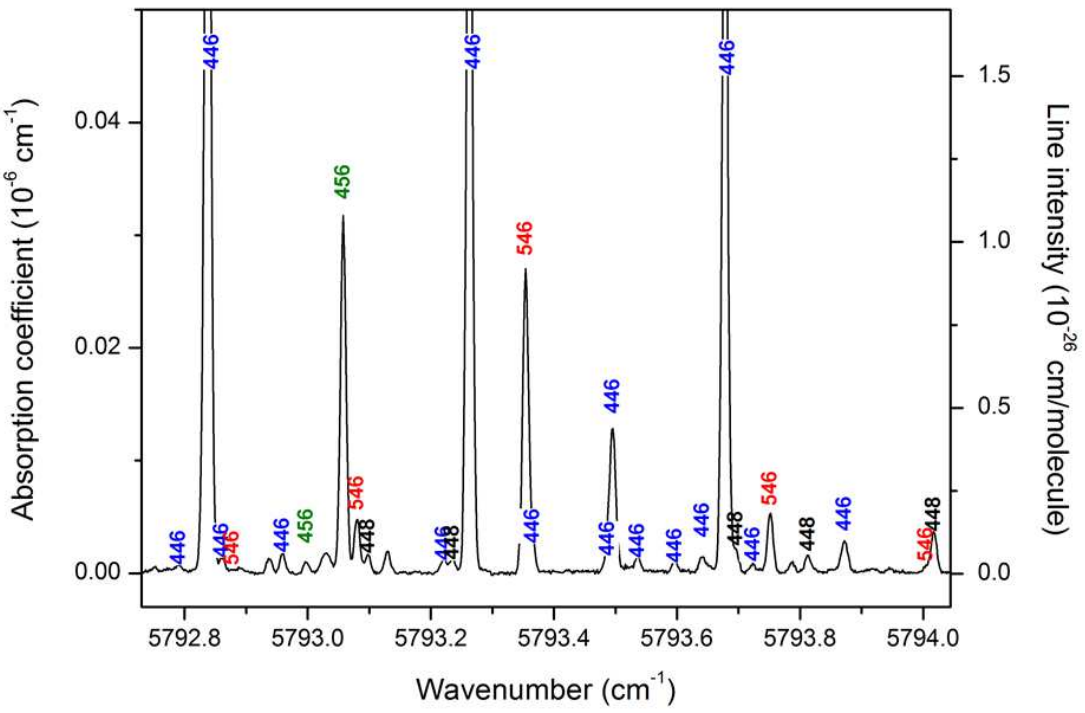

Fig. 4
Example of spectrum interval involving the contribution of four N_2O isotopologues in natural isotopic abundance.

At the final step of the analysis, a total of 3326 transitions could be rovibrationally assigned to 50 bands of the first five nitrous oxide isotopologues, leaving unassigned 984 weak or super weak lines. A sample of spectra involving contributions of four isotopologues is presented in **Fig. 4**. **Table 1** presents the statistics of the assignments. The assigned line list is provided as Supplementary Material. In the case of the principal isotopologue, $^{14}N_2{}^{16}O$, 30 bands were assigned. All but five are newly reported while the observations are significantly extended towards high *J* values for the bands previously reported by FTS (see **Fig. 3**). The four $^{14}N_2{}^{18}O$ and two $^{14}N_2{}^{17}O$ bands are the first ones of these species reported in the studied region.

Table 1
Summary of the number of transitions and bands of different N_2O isotopologues reported in the literature and obtained in this work by CRDS in the 5695 - 5910 cm^{-1} region.

Isotopologue	HITRAN notation	Abundance [13]	Number of bands		Number of transitions
			This work	Literature	
$^{14}N_2{}^{16}O$	446	0.990333	31	5 [19,21-25]	2193
$^{14}N^{15}N^{16}O$	456	3.64093×10^{-3}	5	7 [a] [15]	344
$^{15}N^{14}N^{16}O$	546	3.64093×10^{-3}	8	13 [a] [20]	434
$^{14}N_2{}^{18}O$	448	1.98582×10^{-3}	4	0	310
$^{14}N_2{}^{17}O$	447	3.6928×10^{-4}	2	0	45
		Total	50		3326

Note
[a] Observations using a sample highly isotopically enriched

Fig. 5 shows an overview comparison between the experimental and predicted line lists for each isotopologue. The list of the observed bands is given in **Table 2**. Previous observations in the studied region were all performed by Fourier transform spectroscopy (FTS). The three strongest $^{14}N_2{}^{16}O$ bands (1401-0000, 2311-0110 and 2201-0000 near 5762.37, 5873.3 and 5888.1 cm^{-1}, respectively) are those included in the HITRAN database (see **Fig. 3**). They were first analyzed by Amiot and Guelachvili from spectra recorded with a 60 m absorption path length [21]. The HITRAN line parameters of these bands are those retrieved by Toth using absorption path lengths up to 433 m [22,23]. In addition, Toth reported the 4001-1000 weaker band centered near 5929.8 cm^{-1} which is not included in the HITRAN database. Finally, the 2311-0110 hot band centered at 5737.5 cm^{-1} was analyzed by Wang et al. on the basis of an FTS spectrum recorded with 105 m path length [24]. In the considered region, the 3001-0000 band of $^{14}N^{15}N^{16}O$ and $^{15}N^{14}N^{16}O$ are the only bands of minor isotopologues detected by FTS of natural N_2O [22]. Nevertheless, using samples with a very high isotopic enrichment (>97%) and a path length on the order of 100 m, Ni et al. and

Song et al. reported a large number of bands from their FTS spectra of $^{14}N^{15}N^{16}O$ [15] and $^{15}N^{14}N^{16}O$ [20], respectively. The low isotopic abundance of these isotopologues in our natural sample (about 3.6×10^{-3}) prevented the detection of new bands. As concerned the $^{14}N_2{}^{17}O$ and $^{14}N_2{}^{18}O$ species, the FTS investigation performed by Amiot [25] with highly enriched samples, did not provide observations in our spectral region.

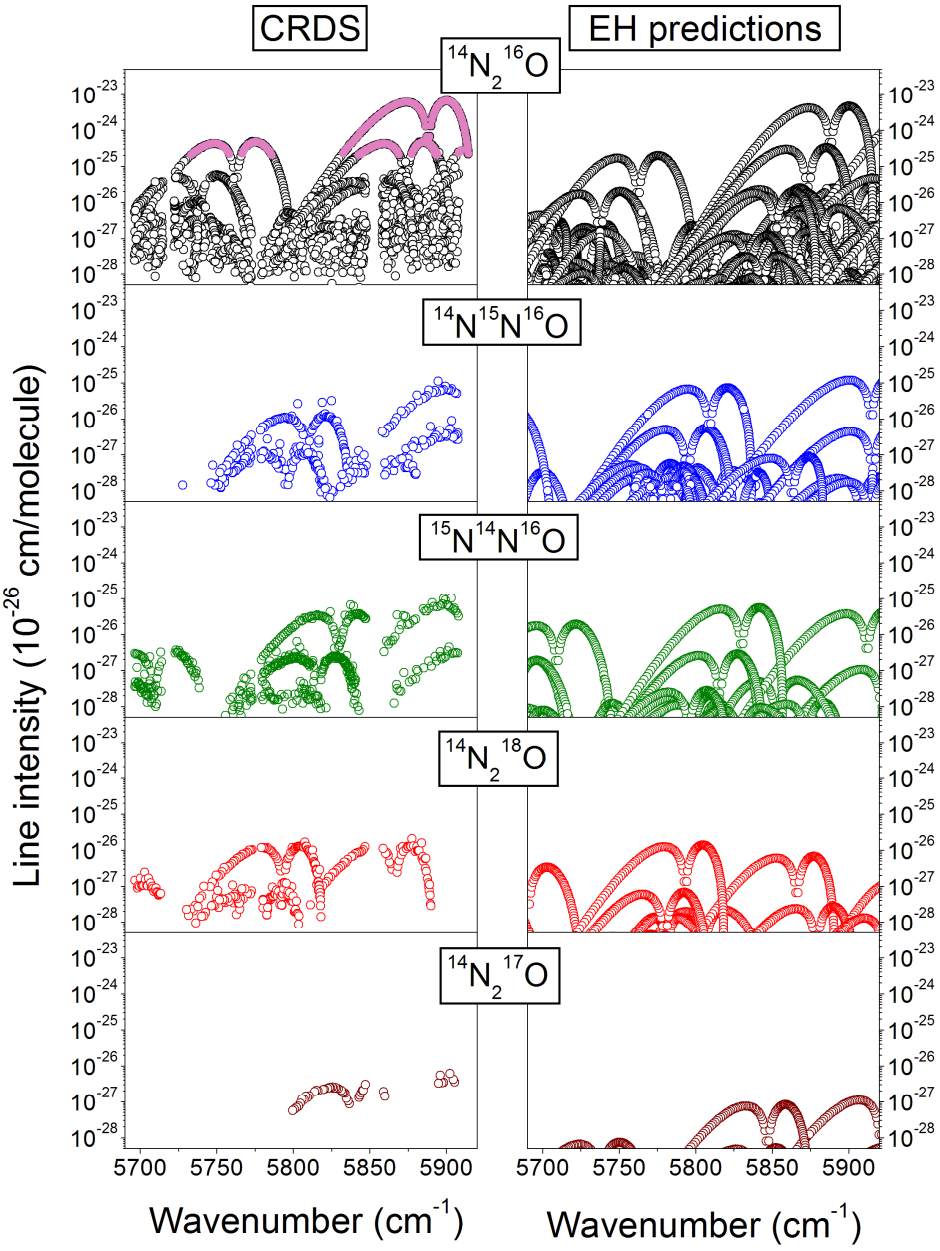

Fig. 5
Overview comparison between the CRDS observations in the 5695-5910 cm^{-1} spectral region and the predictions within the framework of the method of effective operators for the five N_2O isotopologues contributing to the spectrum. Note that there are a few spectral gaps in the experimental line list which could not be covered with the diode lasers at disposal. On the upper panel, the HITRAN line list of $^{14}N_2{}^{16}O$ (pink circles) is superimposed to the corresponding CRDS line list.

4. Band-by-band analysis and rovibrational perturbations

Let us first emphasize that in our region nitrous oxide band assignment in terms of quantum numbers of the harmonic oscillators is ambiguous. There are a number of strong anharmonic and Coriolis resonance interactions in this molecule which lead to a delocalisation of the eigenfunctions in the basis of the harmonic oscillators eigenfunctions. For a given eigenfunction, several harmonic oscillator basis functions can have a large contribution with similar amplitude, leading to ambiguities in the normal mode vibrational labelling. In addition, two or even three eigenfunctions may correspond to the same dominant basis function leading to different vibrational bands with the same normal mode labelling. Moreover the contributions can change strongly with the J rotational quantum number. For the unambiguous assignment of a vibrational state, the $\{P\ \ell_2\ i\}$ triplet is used, where P is a polyad number, ℓ_2 is vibrational angular momentum quantum number. The integer index, i, increasing with energy, numbers the energy levels with the same P and ℓ_2 values, starting with i= 1.

The standard expression of the vibration–rotation energy levels was used for the band-by-band fit of the spectroscopic parameters:

$$F_v(J) = G_v + B_v J(J+1) - D_v J^2(J+1)^2 + H_v J^3(J+1)^3 \quad (1)$$

where G_v is the vibrational term value, B_v is the rotational constant, D_v and H_v are the centrifugal distortion constants, J is the angular momentum quantum number. The lower state constants were constrained to the values obtained by Toth [22,23]. As the e and f sub-bands may be perturbed in a different way, they were fitted independently. The derived constants are listed in **Table 2.** The *rms* values of the differences between the fitted and calculated positions are smaller than 10^{-3} cm^{-1}, which is consistent with our claimed accuracy on line positions. The detailed results of the band-by-band fit of the spectroscopic parameters are provided as Supplementary Materials. For the bands with rotational structure extending above the high energy border of the investigated region (5910 cm^{-1}), the set of line positions used in the fit was complemented with CRDS measurements from Ref. [2] which covers the 5905-6300 cm^{-1} range. In absence of CRDS values (spectral gaps or too strong absorption), we also completed our set of line positions with HITRAN values for the three strongest $^{14}N_2{}^{16}O$ bands [13,23]. The added HITRAN line positions (279 in total) are indicated in the Supplementary Material.

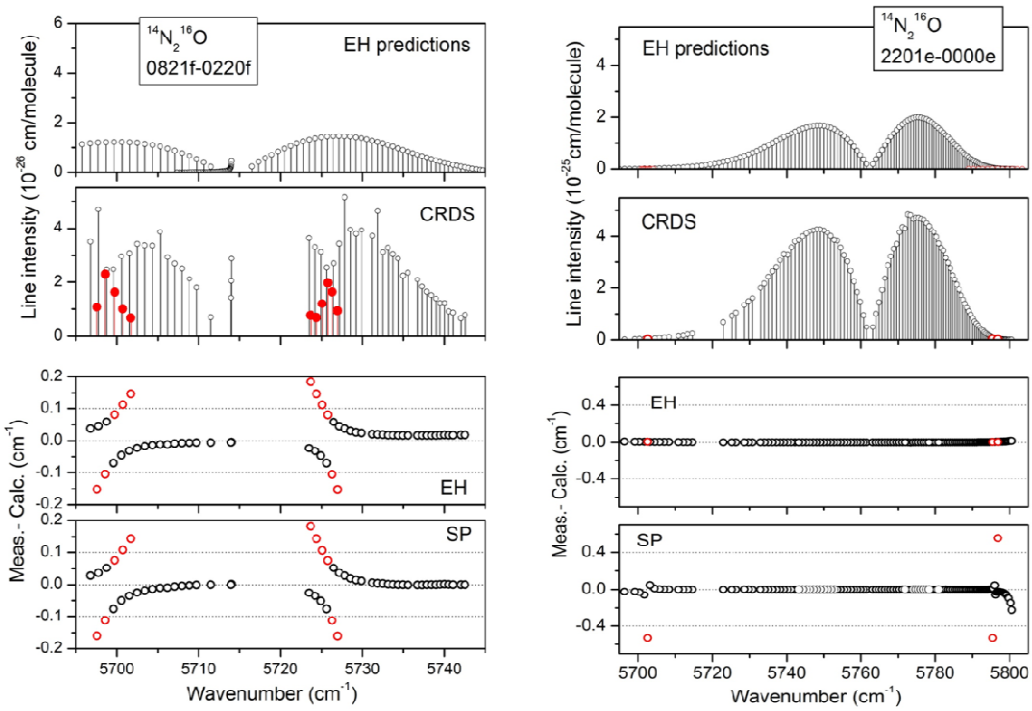

Fig. 6

Resonance coupling in two $^{14}N_2{}^{16}O$ sub-bands leading to local perturbation of line positions and line intensities: 0821f-0220f and 2201e-0000e (left and right hand, respectively). The 0821f upper level (P= 12) is coupled with the 5110f level (P=11) through an interpolyad Coriolis resonance interaction with an energy crossing around J_{cross}= 16 [2]. The 2201e upper level (P= 10) is coupled with the 1820e level (P= 10) through an intrapolyad anharmonic + ℓ-type resonance interaction with an energy crossing around J_{cross}= 56.

From top to bottom:

(i) Predictions of the effective model of $^{14}N_2{}^{16}O$ [14],

(ii) CRDS line list including a number of extra lines (red circles) due to an intensity transfer to the dark state (A number of the strongest lines of the 2201e-0000e band were taken from the HITRAN database),

(iii) Differences between the experimental and EH predicted values of the line positions. As the extra lines of the 0821f-0220f are absent in the effective operator model, the deviations were calculated using the EH predicted positions of the corresponding 0821f-0220f lines,

(iii) Differences between the experimental line positions and the corresponding values computed using the spectroscopic parameters (SP) of the upper state derived in this work (**Table 2**). The plotted shift of the extra lines is relative to the line position calculated with the bright state SP.

A significant number of bands were found to be affected by a local perturbation induced by a resonance vibration-rotation interaction. In those cases, the perturbed line positions were excluded from the fit of the spectroscopic parameters. **Table 3** lists the perturbed bands together with the corresponding perturbers and interaction mechanisms identified on the basis of the effective Hamiltonian model. The value (J_{cross}) of the angular momentum quantum number at which the energy level crossing between bright and dark perturber states takes place is given in the table.. When the coupling involves vibrational states belonging to the same polyad (intrapolyad interaction), the perturbation may be

satisfactorily predicted by the EH model but in two cases, an interpolyad coupling was found responsible of the perturbation. For three bands (0821-0220 and 2201-0000 of $^{14}N_2{}^{16}O$ and 3111-0110 of $^{14}N_2{}^{18}O$), a few extra lines could be identified around the energy crossing lines, using lower state combination relations. **Fig. 6** compares the observations to the EH predictions for the 0821-0220 and 2201-0000 bands of $^{14}N_2{}^{16}O$ affected by inter- and intrapolyad interaction, respectively. As expected, around the energy crossing, the interpolyad interaction induces important shifts of the line positions compared to both the EH predictions and the spectroscopic parameters (SP) calculations. At the opposite, in the case of the intrapolyad interaction of the 2201-0000 band, the EH positions of the perturbed lines are very close to the measurements even for the extra lines.

Table 3 Observed perturbations of the N_2O bands between 5695 - 5910 cm^{-1}

Isotopologue	Band affected	Center (cm^{-1})	Resonance interaction mechanism	J_{cross} [a]	Ref.[b]
$^{14}N_2{}^{16}O$	2201e-0000e	5762.3723	Intrapolyad anharmonic+ℓ-type (10 0 5)↔ (10 2 7) Extra lines: P56 R54 R55	56	
	2221e-0000e	5772.6227	Intrapolyad anharmonic (10 2 9)↔ (10 2 7)	72	
	2311e-0110e	5737.4930	Interpolyad Coriolis (11 1 5)↔ (10 2 20)	smooth	
	1402e-0001e	5774.8275	Intrapolyad anharmonic (14 0 8)↔ (14 0 7)	29	[7]
	3600e-0200e	5861.7095	Intrapolyad anharmonic (12 0 9)↔ (12 0 8)	smooth	
	3221e-0220e 3221f-0220f	5859.2559 5859.2543	Intrapolyad anharmonic (12 2 15)↔ (12 2 16)	smooth	[5]
	3620e-0220e 3620f-0220f	5860.4318 5860.4317	Intrapolyad anharmonic (12 2 16)↔ (12 2 15)	smooth	[5]
	0821e-0220e 0821f-0220f	5714.0247 5714.0255	Interpolyad Coriolis (12 2 12) ↔ (11 1 11) Extra lines: P10 P11 P12 R10 Interpolyad Coriolis (12 2 12) ↔ (11 1 11) Extra lines: P14-P17 R11-R16	10 16	[2]
	0911e-0310e 0911f-0310f	5840.3476 5840.3488	Intrapolyad anharmonic (13 1 8)↔ (13 1 9)	smooth	[5]
$^{14}N^{15}N^{16}O$	1511e-0110e 1511f-0110f	5794.6863 5794.6889	Intrapolyad anharmonic (11 1 6)↔ (11 1 7)	smooth	[15]
$^{15}N^{14}N^{16}O$	0711e-0110e 0711f-0110f	5683.5629 5683.5627	Intrapolyad anharmonic+ℓ-type (11 1 5)↔ (11 3 7)	45 51	
$^{14}N_2{}^{18}O$	3111e-0110e 3111f-0110f	5780.2161 5780.21832	Extra lines: P17 P18 R15 R16 Intrapolyad anharmonic Extra line: P19 Extra lines: P17 P18 R15 R16 Intrapolyad anharmonic (11 1 6)↔ (11 1 7)	smooth smooth	

Notes

[a] Value of the angular momentum quantum number at which the energy level crossing takes place.

[b] Previous reference in which the perturbation of the upper state was observed.

5. Discussion

Fig. 7 shows an overview comparison between the CRDS positions values and the corresponding EH model predictions [8,14-16]. As only few EH parameters of the $^{14}N_2{}^{17}O$ isotopologue were fitted to very restricted number of the line positions [17], this isotopologue is excluded from the comparison.

As expected, the agreement is very good for the $^{14}N^{15}N^{16}O$ and $^{15}N^{14}N^{16}O$ species for which the EH model relies on extensive measurements by FTS of highly enriched samples [15,20]. The average and *rms* values of the (EH-CRDS) position differences are 1.2×10^{-3} and 1.8×10^{-3} cm^{-1} for $^{14}N^{15}N^{16}O$, respectively and 6×10^{-4} and 1.6×10^{-3} cm^{-1} for $^{15}N^{14}N^{16}O$, respectively. Considering the frequent blending and the weakness of the absorption lines of these minor isotopologues in natural abundance in the CRDS spectra, these values are satisfactory. In the case of the main isotopologue, the largest deviations (up to about 0.2 cm^{-1}) are due to the interpolyad perturbation of the 0821f-0220f sub band. Deviations up to 0.035 cm^{-1} are observed for high *J* transitions of the 2311f-0110f sub-band which is also perturbed by interpolyad Coriolis resonance interaction. Excluding 5 % of the measured line positions, the average and *rms* values of the (EH-CRDS) position differences of $^{14}N_2{}^{16}O$ are 3.2×10^{-4} and 4×10^{-3} cm^{-1}, respectively. In the case of $^{14}N_2{}^{18}O$, the set of EH parameters of Ref. [8] was fitted against a scarce set of measured line positions consisting of FTS data below 2435 cm^{-1} and CRDS data in the 6007-8230 cm^{-1} range. The present data provides then a test of the interpolation capabilities of this model. The largest deviations (up to 0.3 cm^{-1}) concern the highly perturbed 1511-0110 hot band near 5780.2 cm^{-1}. The HITRAN line list of $^{14}N_2{}^{18}O$ reproduces the predictions of the effective model [8]. It appears that for a significant part of the measured lines, the deviations largely exceed the HITRAN uncertainty attached to the $^{14}N_2{}^{18}O$ positions (between 0.001 and 0.01 cm^{-1}).

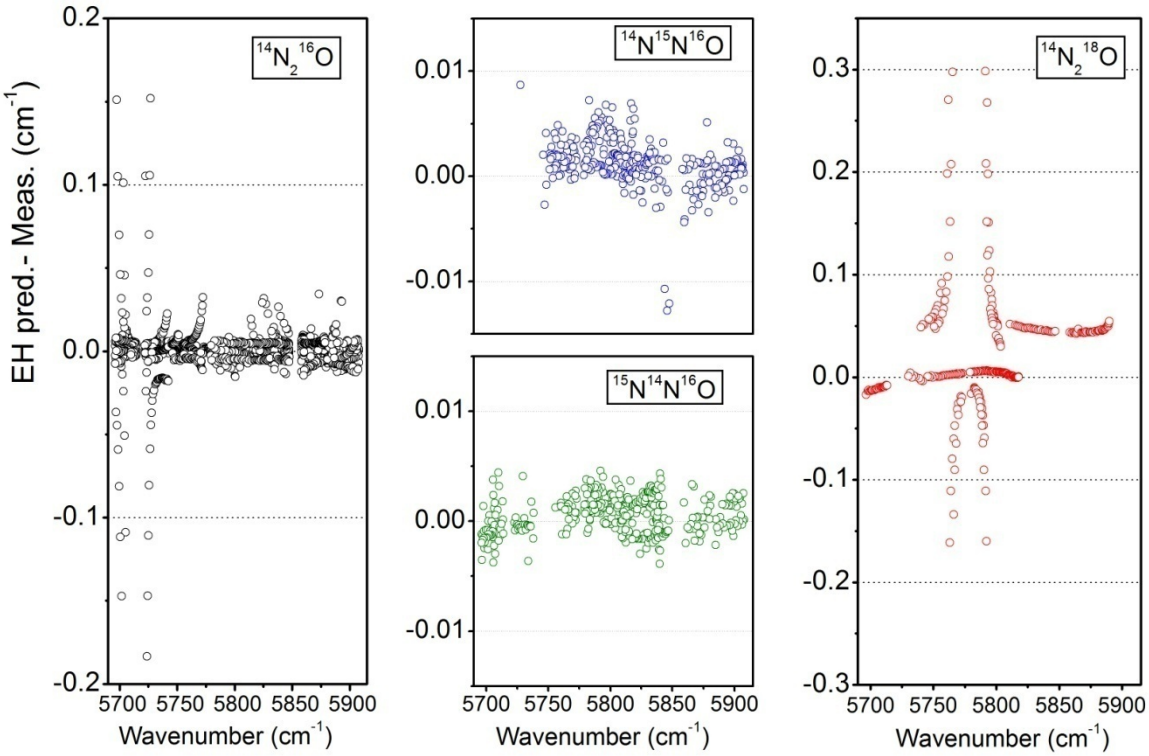

Fig. 7

Differences between the line positions predicted using the effective Hamiltonians [8,14-16] and the measured values, for the first four N_2O isotopologues.

The intensity modeling of the $^{14}N_2{}^{16}O$ spectrum in the region was performed in Ref. [19] on the basis of intensity measurements from Fourier transform spectra. The lines with intensities higher than 5×10^{-26} cm/molecule at 296 K were used to fit the ΔP= 10 EDM parameters. The vibration-rotation eigenfunctions needed to calculate the transition moments corresponded to an old set of EH [26]. The EDM fit of Ref. [19] reached the experimental uncertainties of the line intensities of a few %. Since that time a lot of new experimental line positions were published by CRDS [1-8] and FTS [24]. Part of them (Refs.[1-6,24]) were used to refine the EH parameters of $^{14}N_2{}^{16}O$ [14]. The new set of EH parameters contains a number of additional resonance interaction parameters. Consequently, the expansion coefficients of the eigenfunctions corresponding to the old set [26] and to the new set [14] of EH parameters differ considerably. This is why line intensities computed using the EDM parameters of Ref. [19] and the new eigenfunctions [14] may be inaccurate. This is illustrated in **Fig. 6** where the strong 2201-0000 band near 5762 cm^{-1} is predicted more than two times smaller than measured while it was satisfactorily reproduced in Ref. [19]. In the future, the

line intensities measurements relative to the ΔP=10 series [18,19,22] will be collected and a new set of EDM parameters will be derived using the eigenfunctions of Ref. [14].

As mentioned above, the line intensity predictions were performed for the sake of the line assignments. The $^{14}N_2{}^{18}O$ predicted line list [8] included in the HITRAN2016 database has line intensities computed using the ΔP= 10 EDM parameters of the principal isotopologue [19]. In **Fig. 8,** the comparison of our measured $^{14}N_2{}^{18}O$ line intensities to HITRAN2016 values is presented. As one can see from this figure, the average ratios of the line intensities vary from 0.4 to 1.6. In spite of the low $^{14}N_2{}^{18}O$ natural abundance in our sample (all the measured intensities are smaller than 2×10^{-26} cm/molecule) the present line intensity measurements of $^{14}N_2{}^{18}O$ can be used for the improvement of the line intensity modeling in the ΔP= 10 series of transitions of this isotopologue.

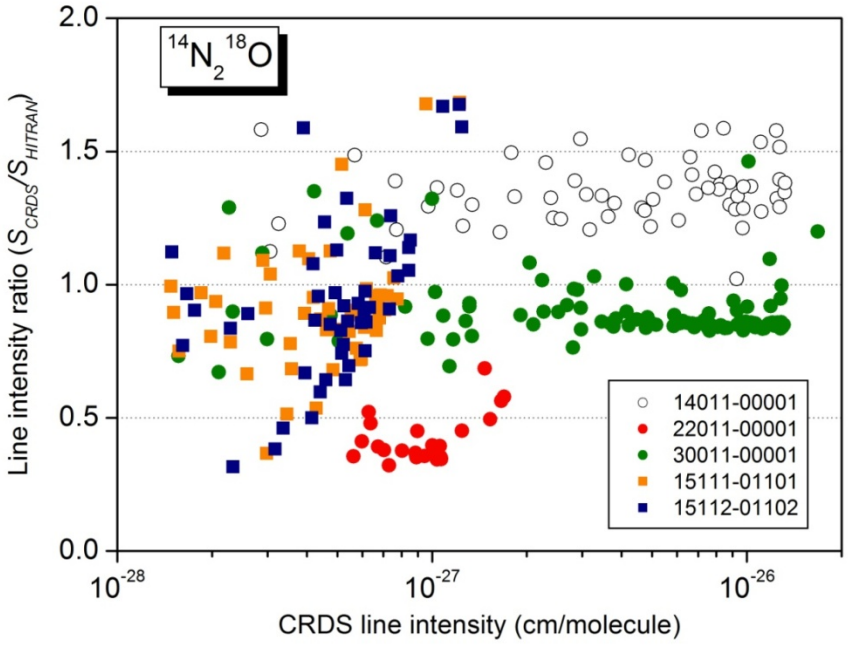

Fig. 8
Ratios of the $^{14}N_2{}^{18}O$ line intensities measured by CRDS to those from HITRAN2016 in the 5695-5910 cm^{-1} region.

6. Concluding remarks

The knowledge of the absorption spectrum of nitrous oxide has been extended by high sensitivity cavity ring down spectroscopy near 1.72 µm. Line parameters were derived for more than 4000 lines with intensities as small as 10^{-28} cm/molecule at 296 K. The line assignment was performed using the predictions within the framework of the method of effective operators. The polyad models of EH were used for the line position and intensity

calculations. Overall, 3326 lines were assigned to 50 bands of five nitrous oxide isotopologues ($^{14}N_2{}^{16}O$, $^{14}N^{15}N^{16}O$, $^{15}N^{14}N^{16}O$, $^{14}N_2{}^{18}O$ and $^{14}N_2{}^{17}O$). 31 bands are newly reported for $^{14}N_2{}^{16}O$, $^{14}N_2{}^{18}O$ and $^{14}N_2{}^{17}O$.

An overall good agreement between the predicted and observed line positions is observed except for two bands - 0821-0220 and 2311-0110 of $^{14}N_2{}^{16}O$ - which are perturbed by interpolyad Coriolis resonance interactions (these interactions are not taken into account by polyad model of EH) and the 3111-0110 band of $^{14}N_2{}^{18}O$ which is perturbed by very strong intrapolyad anharmonic resonance interaction. These results demonstrate once again the importance of interpolyad couplings which make necessary to develop a non-polyad EH model accounting for all interpolyad anharmonic and Coriolis resonance interactions in the $^{14}N_2{}^{16}O$ molecule.

As concerns line intensities, the present study has shown that a new modeling of the line intensities for the $\Delta P = 10$ series of transitions has to be performed. It will be the subject of a separate contribution. The use of an old set of EDM parameters [19] combined with the eigenfunctions corresponding to the most recent EH modeling (that of Ref. [14]) leads to inaccurate line intensity predictions. In general, transition moments have to be computed using consistent sets of EDM parameters and eigenfunctions. This was not the case in the predicted intensities computed in this work in order to help for the rovibrational assignments. Note that, in principle, this issue applies to all the $\Delta P < 10$ series of the Nitrous Oxide Spectroscopy Databank (NOSD) [27] which should be reconsidered.

Acknowledgements

This work is jointly supported by CNRS (France) and RFBR (Russia) in the frame of the International Associated Laboratory SAMIA.

Table 2. Spectroscopic parameters (in cm^{-1}) for the different bands of the N_2O isotopologues assigned in the CRDS spectrum between 5695 and 5910 cm^{-1}. The bands are ordered in increasing order of the upper level vibrational term. Lower state constants were constrained to the values of Refs. [22,23]

Band [a]	$(P\ l_2\ i)$ [b]	G_v(cm^{-1})	B_v (cm^{-1})	D_v($10^{-7}cm^{-1}$)	H_v ($10^{-12}cm^{-1}$)	ν_0 [c](cm^{-1})	J_{max} [d] P/Q/R	N_{fit}/N_{obs} [e]	RMS[f]	Note[g]
$^{14}N_2{}^{16}O$ isotopologue										
0911e-0310e	*(13 1 6)*	7441.4424(22)	0.4146795(55)			5692.3772(22)	R32	7/21	0.20	
0911f-0310f	*(13 1 6)*	7441.4394(44)	0.417529(15)	1.76(12)		5692.3743(44)	R27	7/18	0.37	
0821e-0220e	*(12 2 12)*	6891.76938(33)	0.4162658(21)	-0.968(32)	-29.2(13)	5714.02471(33)	P19/R40	21/47	0.55	1
0821f-0220f 0821f-0220e	*(12 2 12)*	6891.77018(35)	0.4163114(25)	3.118(36)	17.1(13)	5714.02551(51)	P19/R42 Q4	18/42 3/3	0.68	
0801e-0200e	(12 0 7)	6882.69176(16)	0.4160533(11)	5.932(18)	35.67(74)	5714.55947(16)	P20/R40	49/50	0.47	
3310e-0000e	*(9 1 9)*	5722.82400(14)	0.41304592(51)	1.4034(39)	1.535(80)	5722.82400(14)	P26/R57	65/66	0.47	
3310f-0000e	*(9 1 9)*	5722.82471(27)	0.41466683(83)	0.9703(29)		5722.82471(27)	Q56	20/21	0.81	
2311f-0110f 2311f-0110e	(11 1 5)	6323.26014(13)	0.41695852(28)	2.7347(12)		5737.49227(13)	P42/R52 Q23	78/78 12/12	0.64	
2311e-0110e 2311e-0110f	(11 1 5)	6323.26091(11)	0.41471051(32)	2.5276(22)	3.122(36)	5737.49304(11)	P40/R68 Q30	77/85 23/24	0.58	2
3201e-1000e	*(12 0 8)*	7024.09232(24)	0.4136322(97)	3.8029(96)	14.01(25)	5739.18898(24)	P43/R51	67/68	0.79	
3420f-0110f	*(10 2 20)*	6330.51680(25)	0.41449164(77)	1.2713(43)		5744.74893(25)	P21/R43	30/31	0.62	
2201e-0000e	*(10 0 5)*	5762.372287(90)	0.41547889(41)	3.7830(43)	13.08(12)	5762.372287(90)	P61/R75	93/121	0.40	3,4
2221e-0000e	*(10 2 9)*	5772.62270(31)	0.4157353(13)	0.390(14)	-10.60(43)	5772.62270(31)	P66/R68	65/98	0.64	5
1402e-0001e	*(14 0 8)*	7998.58431(40)	0.4095846(78)	3.02(38)	435(51)	5774.82754(40)	P26/R24	28/29	0.65	6
3400e-0110e	*(10 0 12)*	6370.30688(49)	0.4123503(21)	0.580(21)	6.71(60)	5784.53901(49)	P49/R43	32/34	0.7	
4111e-1110e 4111e-1110f	*(13 1 10)*	7715.06419(15)	0.41075732(47)	1.9471(24)		5834.79845(15)	P54/R17 Q2	44/48 0/2	0.57	
4111f-1110f	*(13 1 10)*	7715.06426(19)	0.41260094(61)	1.9706(32)		5834.79852(19)	P49/R16	46/48	0.73	
0911e-0310e* 0911e-0310f*	*(13 1 8)*	7589.41280(45)	0.4131845(92)	4.751(63)		5840.34757(45)	P50/R44 Q3	15/49 1/2	0.85	7
0911f-0310f* 0911f-0310e*	*(13 1 8)*	7589.41399(47)	0.415699(11)	10.69(51)		5840.34876(47)	P47/R47 Q6	16/55 0/2	0.58	
3331e-0330e	*(13 3 16)*	7613.28051(42)	0.4147258(61)	3.31(21)	477(20)	5846.36813(42)	P28/R26 Q24	26/29 6/8	0.79	
3331e-0330f										
3331f-0330f	*(13 3 16)*	7613.28085(36)	0.4147142(57)	2.67(22)	400(23)	5846.36861(36)	P32/R29 Q24	25/34 6/8	0.66	
3331f-0330e										
4001e-1000e	*(12 0 10)*	7137.12699(14)	0.41096998(42)	2.3449(13)	2.499(58)	5852.22365(14)	P58/R59	92/94	0.48	
3201e-0200e	*(12 0 8)*	7024.09255(21)	0.41363178(87)	3.8052(85)	14.12(22)	5855.96025(21)	P58/R53	81/88	0.69	

3221f-0220f 3221f-0220e	*(12 2 15)*	7036.99892(47)	0.416088(15)	61.3(12)	6950(240)	5859.25425(47)	P60/R56 Q15	19/80 8/11	0.76	8
3221e-0220e 3221e-0220f	*(12 2 15)*	7037.00052(49)	0.416011(15)	53.5(11)	5760(240)	5859.25585(49)	P59/R54 Q15	14/79 8/14	0.60	
3002e-0001e	*(14 0 9)*	8083.95490(35)	0.40717926(92)	1.2906(49)		5860.19814(35)	P46/R37	29/35	0.77	
3620e-0220e 3620e-0220f	*(12 2 16)*	7038.17650(63)	0.418067(21)	-58.0(13)	-5310(220)	5860.43183(63)	P34/R30 Q9	13/36 3/5	0.85	9
3620f-0220f 3620f-0220e	*(12 2 16)*	7038.17639(45)	0.418101(14)	-48.5(11)	-5610(21)	5860.43172(45)	P33/R33 Q9	12/35 5/5	0.63	
3600e-0200e	*(12 0 9)*	7029.84176(44)	0.4198935(31)	12.877(59)	161.9(31)	5861.70946(44)	P42/R39	33/38	0.81	10
3111e-0110e 3111e-0110f	*(11 1 6)*	6459.06943(11)	0.41261160(31)	2.0820(19)	1.296(31)	5873.30156(11)	P69/R59 Q39	119/119 23/25	0.63	4
3111f-0110f 3111f-0110e	*(11 1 6)*	6459.06975(12)	0.41431089(31)	2.1480(17)	0.980(24)	5873.30188(12)	P72/R68 Q33	129/132 19/21	0.70	
3510f-0110f 3510f-0110e	(11 1 7)	6466.52762(24)	0.4216829(18)	4.455(30)	-10.1(10)	5880.75975(24)	P48/R29 Q5	40/43 4/4	0.78	
3510e-0110e 3510e-0110f	*(11 1 7)*	6466.52930(22)	0.4179790(12)	4.000(16)	17.07(54)	5880.76143(22)	P47/R32 Q6	41/45 3/4	0.64	
1401e-0000e	*(10 0 6)*	5888.106124(93)	0.41292884(19)	2.36206(89)	2.020(11)	5888.106124(93)	P45-P85	113/35	0.51	4,11
3401e-2000e	*(14 0 15)*	8452.63461(93)	0.4090440(55)	0.455(67)		5889.29517(93)	P15/R26	11/13	0.77	
0(10)00e-0000e	*(10 0 7)*	5902.96649(21)	0.4196587(13)	9.028(16)	83.73 (48)	5902.96626(16)	P41/R05	55/74	0.84	11
0(10)20e-0000e	*(10 2 11)*	5905.41181(55)	0.41367383(99)	1.1996(48)	-2.978(66)	5905.41181(55)	P71/R65	67/82	1.09	11
3201e-1000e*	*(12 0 12)*	7214.67678(16)	0.40962698(62)	1.0465(55)	5.91(13)	5929.77344(16)	P56/R53	87/98	0.65	11
3311e-1110e	*(13 1 12)*	7817.83064(26)	0.40971487(83)	1.2850(46)		5937.56490(26)	P41/R42	46/55	0.91	11
3311f-1110f	*(13 1 12)*	7817.83126(27)	0.41130070(92)	0.9331(59)		5937.56552(27)	P40/R40	48/57	0.89	
4001e-0200e	*(12 0 10)*	7137.12707(17)	0.41096960(61)	2.3530(50)	2.80(11)	5968.99477(17)	P59/R44	71/81	0.65	11
3001e-0000e	*(10 0 8)*	5974.844663(78)	0.41067465(18)	1.41265(88)	2.125(11)	5974.844663(78)	P53-P79	132/137	0.42	4,11
2311f-0110f* 2311f-0110e*	*(11 1 8)*	6567.76776(16)	0.41223858(44)	1.3339(27)	1.520(43)	5981.99989(16)	P69/R61 Q35	89/108 22/23	0.78	11
2311e-0110e* 2311e-0110f*	*(11 1 8)*	6567.76809(18)	0.41097052(53)	1.5181(37)	0.687(69)	5982.00022(18)	P63/R61 Q29	82/94 20/23	0.81	
$^{14}N^{15}N^{16}O$ isotopologue										
1511f-0110f	*(11 1 6)*	6370.12469(82)	0.415176(23)	25.4(13)		5794.69104(82)	P44/R49	18/70	0.91	12
1511e-0110e 1511e-0110f	*(11 1 6)*	6370.12105(49)	0.413306(18)	21.0(11)		5794.68740(49)	P42/R49 Q3	19/66 1/2	0.96	
2201e-0000e	*(10 0 6)*	5808.92973(14)	0.41301161(58)	2.5987(43)		5808.92973(14)	P54/R54	90/92	0.56	

4001e-1000e	*(12 0 12)*	7143.39717(46)	0.4085025(17)	1.421(12)		5863.04305(46)	P37/R29	25/28	0.83	
3001e-0000e	*(10 0 8)*	5914.70755(21)	0.41017181(73)	1.6592(58)	0.86(12)	5914.70755(21)	P64/R51	88/100	0.92	11
3111f-0110f	*(11 1 8)*	6491.00794(30)	0.41154694(93)	1.5524(52)		5915.57429(30)	P46/R38	40/48	0.94	11
3111e-0110e	*(11 1 8)*	6491.00858(30)	0.41043667(69)	1.6644(22)		5915.57493(30)	P58/R31	34/43	0.95	
$^{15}N^{14}N^{16}O$ isotopologue										
0711e-0110e	*(11 1 5)*	6268.8790(13)	0.4007162(27)	2.165(12)		5683.5668(13)	R42	18/20	0.93	13
0711f-0110f	*(11 1 5)*	6268.87486(70)	0.4028018(15)	2.3796(64)		5683.56274(70)	R44	13/16	0.55	
2201e-0000e	*(10 0 5)*	5709.25068(16)	0.40142497(98)	3.213(13)	9.04(42)	5709.25068(16)	P15/R45	40/45	0.52	
4001e-1000e	*(12 0 10)*	7065.52427(36)	0.3971431(14)	2.0211(95)		5795.63229(36)	P32/R39	27/31	0.91	
3201e-0200e	*(12 0 8)*	6957.89997(46)	0.3996484(30)	3.122(43)	8.0(15)	5797.92826(46)	P33/R43	27/28	0.83	
3111f-0110f	*(11 1 6)*	6400.85373(11)	0.40037223(25)	1.9091 (10)		5815.54161(11)	P51/R52	69/75	0.48	
3111e-0110e	*(11 1 6)*	6400.85382(13)	0.39878792(36)	1.8492(17)		5815.54170(13)	P49/R51	71/76	0.58	
3001e-0000e	*(10 0 8)*	5911.94548(22)	0.39725038(98)	1.2021(90)	2.08(21)	5911.94548(22)	P46/R55	70/85	0.93	11
1401e-0000e	*(10 0 6)*	5829.909549(87)	0.39901775(32)	2.1455(24)	1.703(46)	5829.909549(87)	P63/R26	79/79	0.40	
2311f-0110f	*(11 1 8)*	6507.10800(31)	0.39876092(73)	1.1353(32)		5921.79588(31)	P49/R48	43/51	0.93	11
2311e-0110e	*(11 1 8)*	6507.10855(29)	0.39749753(81)	1.3469(41)		5921.79643(29)	P47/R41	44/55	0.90	
$^{14}N_2{}^{17}O$ isotopologue										
3001e-0000e	*(10 0 6)*	5838.86886(15)	0.40066286(78)	2.1529(60)		5838.86886(15)	P38/R34	38/38	0.51	
2201e-0000e	*(10 0 8)*	5917.0005(28)	0.399806(20)	4.45(30)		5917.0005(28)	P23	7/7	0.62	
$^{14}N_2{}^{18}O$ isotopologue										
1401e-0000e	*(10 0 5)*	5690.2279(28)	0.4024422(65)	1.617(36)		5690.2279(28)	R34	13/26	0.49	
3111e-0110e 3111e-0110f	*(11 1 6)*	6364.44072(76)	0.389676(19)	4.07(25)	91.8(88)	5780.21606(76)	P39/R38 Q5	10/52 1/2	0.68	14
3111f-0110f 3111f-0110e	*(11 1 6)*	6364.44298(58)	0.3909966(25)	1.504(14)		5780.21832(58)	P43/R41 Q1	10/55 1/1	0.85	
3001e-0000e	*(10 0 6)*	5793.237645(98)	0.38956118(32)	2.0278(25)	2.013(51)	5793.237645(98)	P56/R60	100/103	0.47	
2201e-0000e	*(10 0 8)*	5866.05649(12)	0.38899493(45)	0.8171(42)	2.70(10)	5866.05649(12)	P50/R53	68/70	0.43	

[a] $V_1V_2\ell_2\ V_3$correspond to the maximum value of the modulo of the expansion coefficients of the eigenfunction. V_2 is given between parentheses when it is larger than 10.
* The asterisk is used to distinguish the different upper vibrational states with the same labelling in terms of the harmonic oscillators quantum numbers
[b] Cluster labeling notation: ($P=2V_1+V_2+4V_3$, ℓ_2,i): i is the order number within the cluster, increasing with the energy.
[c] v_0 is the band center
[d] Observed branch with the maximum value of the total angular momentum quantum number.
[e] n is number of transitions included in the fit; N is number of assigned transitions.
[f] Root Mean Squares of residuals of the spectroscopic parameters fit is given in 10^{-3} cm^{-1}.
[g] *Notes*:
1 - Interpolyad Coriolis resonance interaction (12 2 12) ↔ (11 1 11) (energy levels crossing at e: J=10; f: J= 16)

2 - Interpolyad Coriolis resonance interaction (11 1 5) ↔ (10 2 20) (energy levels crossing: smooth)
3 - Intrapolyad anharmonic+ℓ-type (10 0 5)↔ (10 2 7) (energy levels crossing at J= 56)
4 – Line positions given the HITRAN2016 database [13] were included in the fit (See Supplementary Material)
5 - Intrapolyad anharmonic resonance interaction (10 2 9) ↔ (10 2 7) (energy levels crossing at J= 72)
6 - Intrapolyad anharmonic resonance interaction (14 0 8) ↔ (14 0 7) (energy levels crossing at J= 29)
7 - Intrapolyad anharmonic resonance interaction (13 1 8) ↔ (13 1 9)) (smooth energy levels crossing)
8 - Intrapolyad anharmonic resonance interaction (12 2 15) ↔ (12 2 16) (smooth energy levels crossing)
9 - Intrapolyad anharmonic resonance interaction (12 2 16) ↔ (12 2 15) (smooth energy levels crossing)
10 - Intrapolyad anharmonic resonance interaction (12 0 9) ↔ (12 0 8) (smooth energy levels crossing)
11- Line positions above 5908 cm^{-1} were taken from Ref. [2] and included in the fit (See Supplementary Material)
12- Intrapolyad anharmonic resonance interaction (11 1 6) ↔ (11 1 7)) (smooth energy levels crossing)
13- Intrapolyad anharmonic+ℓ-type (11 1 5)↔ (11 3 7) (energy levels crossing at e: J=45; f: J=51)
14- Intrapolyad anharmonic resonance interaction (11 1 6) ↔ (11 1 7) (smooth energy levels crossing)

References

1. Liu AW, Kassi S, Malara P, Romanini D, Perevalov VI, Tashkun SA, Hu SM, Campargue A. High sensitivity CW-cavity ring down spectroscopy of N_2O near 1.5l μm (I). J Mol Spectrosc 2007:244;33-47.
2. Liu AW, Kassi S, Perevalov VI, Tashkun SA, Campargue A. High sensitivity CW-cavity ring down spectroscopy of N_2O near 1.5l μm (II). J Mol Spectrosc 2007:244;48-62.
3. Liu AW, Kassi S, Perevalov VI, Hu SM, Campargue A. High sensitivity CW-cavity ring down spectroscopy of N_2O near 1.5 μm (III). J Mol Spectrosc 2009;254:20–7.
4. Liu AW, Kassi S, Perevalov VI, Tashkun SA, Campargue A. High sensitivity CW-Cavity Ring Down Spectroscopy of N_2O near 1.28 μm. J Mol Spectrosc 2011;267:191-9.
5. Lu Y, Mondelain D, Liu AW, Perevalov VI, Kassi S, Campargue A. High Sensitivity *CW*-Cavity Ring Down Spectroscopy of N_2O between 6950 and 7653 cm^{-1} (1.44-1.31 μm): I. Line positions. J Quant Spectrosc Radiat Transfer 2012;113:749-62.
6. Karlovets EV, Lu Y, Mondelain D, Kassi S, Campargue, Tashkun SA, Perevalov VI, High sensitivity CW-Cavity Ring Down Spectroscopy of N_2O between 6950 and 7653 cm^{-1} (1.44–1.31 μm): II. Line intensities. J Quant Spectrosc Radiat Transfer 2013;117:81–7.
7. Karlovets EV, Campargue A, Kassi S, Perevalov VI, Tashkun SA. High sensitivity Cavity Ring Down Spectroscopy of N_2O near 1.22 μm: (I) Rovibrational assignments and band-by-band analysis. J Quant Spectrosc Radiat Transfer 2016;169:36–48.
8. Tashkun SA, Perevalov VI, Karlovets EV, Kassi S, Campargue A. High sensitivity Cavity Ring Down Spectroscopy of N_2O near 1.22 μm: (II) $^{14}N_2{}^{16}O$ line intensity modeling and global fit of $^{14}N_2{}^{18}O$ line positions. J Quant Spectrosc Radiat Transfer 2016;176:62–69. 10.1016/j.jqsrt.2016.02.020
9. Kassi S, Campargue A. Cavity ring down spectroscopy with 5×10^{-13} cm^{-1} sensitivity. J Chem Phys 2012;137:234201. doi: 10.1063/1.4769974
10. Čermák P, Karlovets EV, Mondelain D, Kassi S, Perevalov VI, Campargue A. High sensitivity CRDS of CO_2 in 1.74 μm transparency window. A validation test for the spectroscopic databases. J Quant Spectrosc Radiat Transf 2018;207:95–103.
11. Karlovets EV, Čermák P, Mondelain D, Kassi S, Campargue A, Tashkun SA, Perevalov VI. Analysis and theoretical modelling of the ^{18}O enriched carbon dioxide spectrum by CRDS near 1.74 μm. J Quant Spectrosc Radiat Transf 2018;217:73–85.
12. Karlovets EV, Sidorenko AD, Čermák P, Mondelain D, Kassi S, Perevalov VI, Campargue A. The $^{13}CO_2$ absorption spectrum by CRDS near 1.74 μm. J Mol Spectrosc 2018;354:54-59. 10.1016/j.jms.2018.10.003
13. Gordon IE, Rothman LS, Hill C, Kochanov RV, Tan Y, Bernath PF, Birk M, Boudon V, Campargue A, Chance KV, Drouin BJ, Flaud J-M, Gamache RR, Hodges JT, Jacquemart D, Perevalov VI, Perrin A, Shine KP, Smith MAH, Tennyson J, Toon GC, Tran H, Tyuterev VlG, Barbe A, Császár AG, Devi VM, Furtenbacher T, Harrison JJ, Hartmann J-M, Jolly A, Johnson TJ, Karman T, Kleiner I, Kyuberis AA, Loos J, Lyulin OM, Massie ST, Mikhailenko SN, Moazzen-Ahmadi N, Müller HSP, Naumenko OV, Nikitin AV, Polyansky OL, Rey M, Rotger M, Sharpe SW, Sung K, Starikova E, Tashkun SA, Vander Auwera J, Wagner G, Wilzewski J, Wcisło P, Yu S, Zak EJ. The HITRAN2016 molecular spectroscopic database. J Quant Spectrosc Radiat Transfer 2017;203:3-69. doi: 10.1016/j.jqsrt.2017.06.038
14. Perevalov VI, Tashkun SA, Kochanov RV, Liu AW, Campargue A, Global modeling of the line positions of $^{14}N_2{}^{16}O$ within the framework of the polyad model of effective Hamiltonian. J Quant Spectrosc Radiat Transf 2012;113:1004-12.
15. Ni HY, Song KF, Perevalov VI, Tashkun SA, Liu AW, Wang L, Hu SM. Fourier-transform spectroscopy of $^{14}N^{15}N^{16}O$ in the 3800-9000 cm^{-1} region and global modelling of its absorption spectrum. J Mol Spectrosc 2008;248:41–60.
16. Tashkun SA, Perevalov VI, Kochanov RV, Liu AW, Hu SM. Global fittings of $^{14}N^{15}N^{16}O$ and $^{15}N^{14}N^{16}O$ vibrational–rotational line positions using the effective Hamiltonian approach. J Quant Spectrosc Radiat Transfer 2010;210:1089-1105.

17. Vlasova AV, Perevalov BV, Tashkun SA, Perevalov VI. Global fittings of the line positions of the rare isotopic species of the nitrous oxide molecule. In: Proceedings of the XVth symposium on high-resolution molecular spectroscopy, Nizhny Novgorod, Russia, vol. 6580. SPIE; 2006. p. 658007.
18. Daumont L, Vander Auwera J, Teffo JL, Perevalov VI, Tashkun SA. Line intensity measurements in $^{14}N_2{}^{16}O$ and their treatment using the effective dipole moment approach. I. The 4300–5200 cm^{-1} region. J Mol Spectrosc 2001;208:281-291.
19. Daumont L, Vander Auwera J, Teffo JL, Perevalov VI, Tashkun SA. Line intensity measurements in $^{14}N_2{}^{16}O$ and their treatment using the effective dipole moment approach. II. The 5400–11,000 cm^{-1} region. J Quant Spectrosc Radiat Transfer 2007;104:342–56.
20. Song KF, Liu AW, Ni HY, Hu SM. Fourier-transform spectroscopy of $^{15}N^{14}N^{16}O$ in the 3500-9000 cm^{-1} region J Mol Spectrosc 2009;255:24–31.
21. Amiot C, Guelachvili G. Vibration-rotation bands of $^{14}N_2{}^{16}O$: 1.2 micron-3.3 micron region. J Mol Spectrosc 1974;51:475-91.
22. Toth RA. Line positions and strengths of N_2O between 3515 and 7800 cm^{-1}. J Mol Spectrosc 1999;197:158-87.
23. R.A. Toth, http://mark4sun.jpl.nasa.gov/n2o.html
24. Wang L, Perevalov VI, Tashkun SA, Gao B, Hao LY, Hu SM. Fourier transform spectroscopy of N_2O weak overtone transitions in the 1–2 μm region. J Mol Spectrosc 2006:237;129-36.
25. Amiot C. Vibration-rotation bands of $^{15}N_2{}^{16}O$-$^{14}N_2{}^{18}O$. J Mol Spectrosc 1976;59:380-95.
26. Perevalov VI, Tashkun SA, Teffo JL. Global fittings of rovibrational line positions of nitrous oxide, in: Program and Abstract of Sixteen Colloquium on High Resolution Molecular Spectroscopy (Université de Bourgogne, Dijon, 1999). P.3.
27. Tashkun SA, Perevalov VI, Lavrentieva NN. NOSD-1000, the high-temperature nitrous oxide spectroscopic databank. J Quant Spectrosc Radiat Transf 2016; 177 :43–48. doi.org/10.1016/j.jqsrt.2015.11.014i.

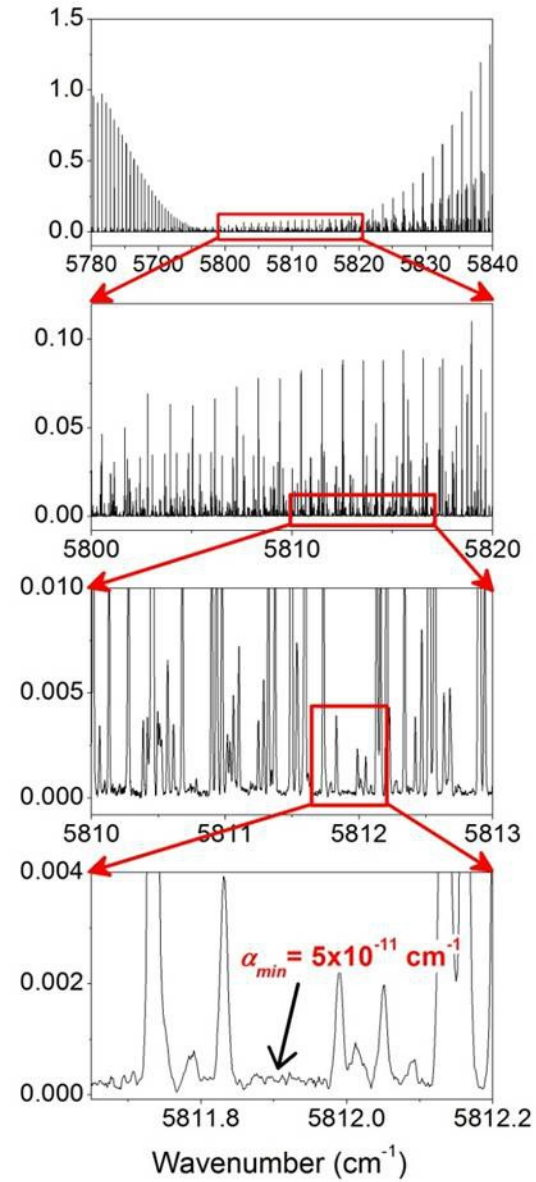
1.5
1.0
0.5
0.0
5780 5790 5800 5810 5820 5830 5840
0.10
0.05
0.00
5800 5810 5820
0.010
0.005
0.000
5810 5811 5812 5813
0.004
0.002
0.000
α_{min} = 5x10^{-11} cm^{-1}
5811.8 5812.0 5812.2
Wavenumber (cm^{-1})

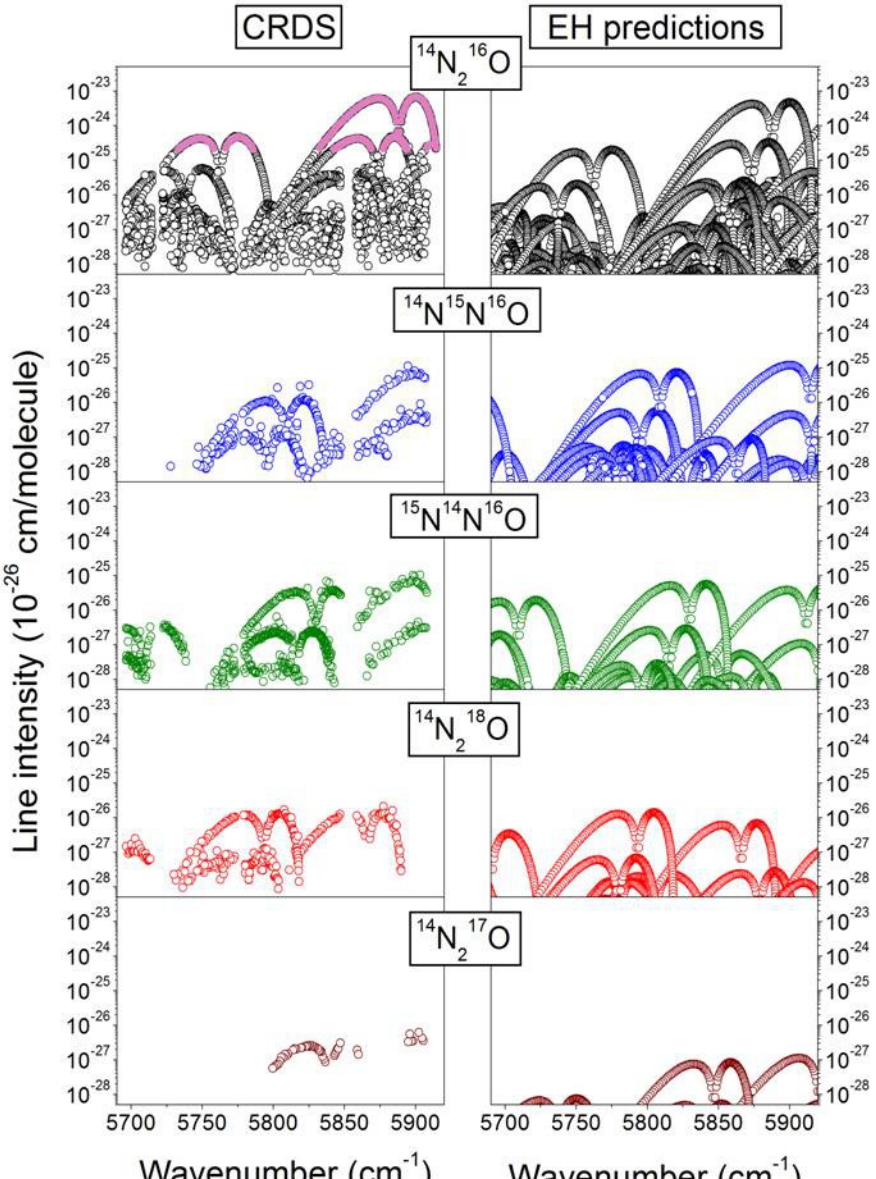
CRDS
EH predictions
$^{14}N_2{}^{16}O$
$^{14}N^{15}N^{16}O$
$^{15}N^{14}N^{16}O$
$^{14}N_2{}^{18}O$
$^{14}N_2{}^{17}O$
Line intensity (10^{-26} cm/molecule)
10^{-23} 10^{-24} 10^{-25} 10^{-26} 10^{-27} 10^{-28}
5700 5750 5800 5850 5900
Wavenumber (cm^{-1})
Wavenumber (cm^{-1})